SUPPLEMENTAL FIGURES and LEGENDS

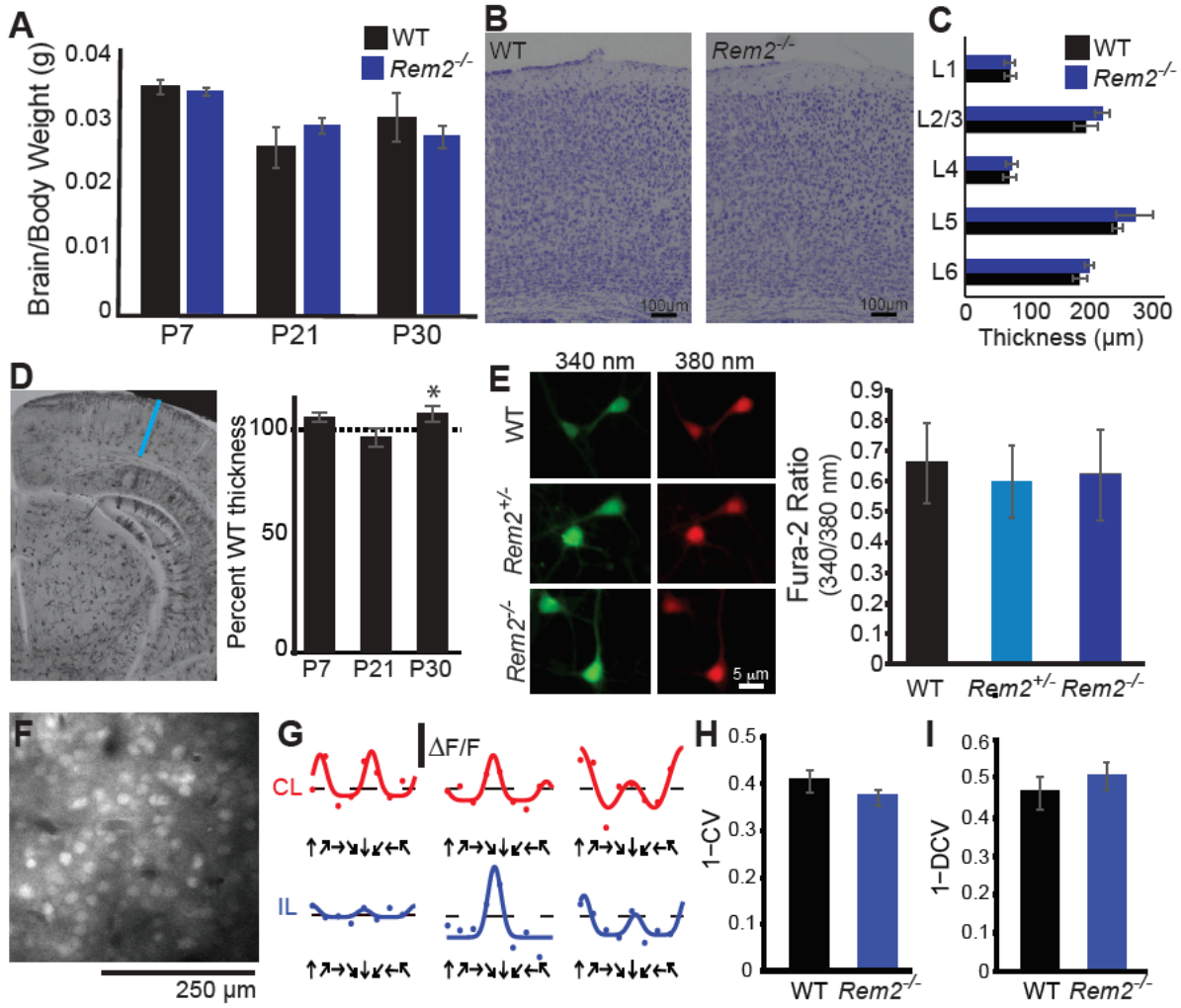

Figure S1 related to Figure 2: *Rem2*$^{-/-}$ mice display no gross anatomical or function cortical abnormalities. **A**) Brain/body weight ratio of P7, P21 and P30 WT and *Rem2*$^{-/-}$ mice. **B**) Representative images of WT and *Rem2*$^{-/-}$ Nissl stained brain slices from P16 mice (30 μm sections, scale bar 100 μm). **C**) Cortical layer thickness measured in P16 WT and *Rem2*$^{-/-}$ mice (N=3 animals per condition). **D**) (Left) Representative image of visual cortex of P21 mouse brain stained with Golgi-Cox labeling. Blue line shows the distance of cortical thickness measured from the deep extent of L6 to the pial surface. (Right) Percent cortical thickness measured in P7 (N=2 animals per condition), P21 (N=3 animals per condition), and P30 mice (N=4 animals per condition). Data is presented as percent thickness of *Rem2*$^{-/-}$ to WT cortical thickness. *$p < 0.05$ by student's *t*-test. **E**) (Left) Representative images of Fura-2 calcium acquired at 340 nm (green) and 380 nm (red) in WT, *Rem2*$^{+/-}$, or *Rem2*$^{-/-}$ cultured neurons. (Right) The ratio of Fura-2 signal (340 nm/380 nm) measured in WT, *Rem2*$^{+/-}$, or *Rem2*$^{-/-}$ cultured cortical neurons. **F**) Representative imaging field of neurons in mouse binocular visual cortex loaded with the calcium indicator dye Oregon Green BAPTA-1AM. Scale bar, 250 μm. **G**) Example responses of 3 cells to visual stimulation (represented as ΔF/F, black vertical bar) of the contralateral (C) eye (top; red lines) and ipsilateral (I) eye (bottom; blue lines) with drifting gratings moving in different directions (black arrows). **H**) Orientation selectivity as assessed by circular variance (1-CV) for WT (n=59 cells, N=7 animals) and *Rem2*$^{-/-}$ mice (n=82 cells; N=5 animals). **I**) Direction selectivity as assessed by circular variance in direction space (1-DCV) for WT and *Rem2*$^{-/-}$ mice. All data is presented as mean ± SEM.

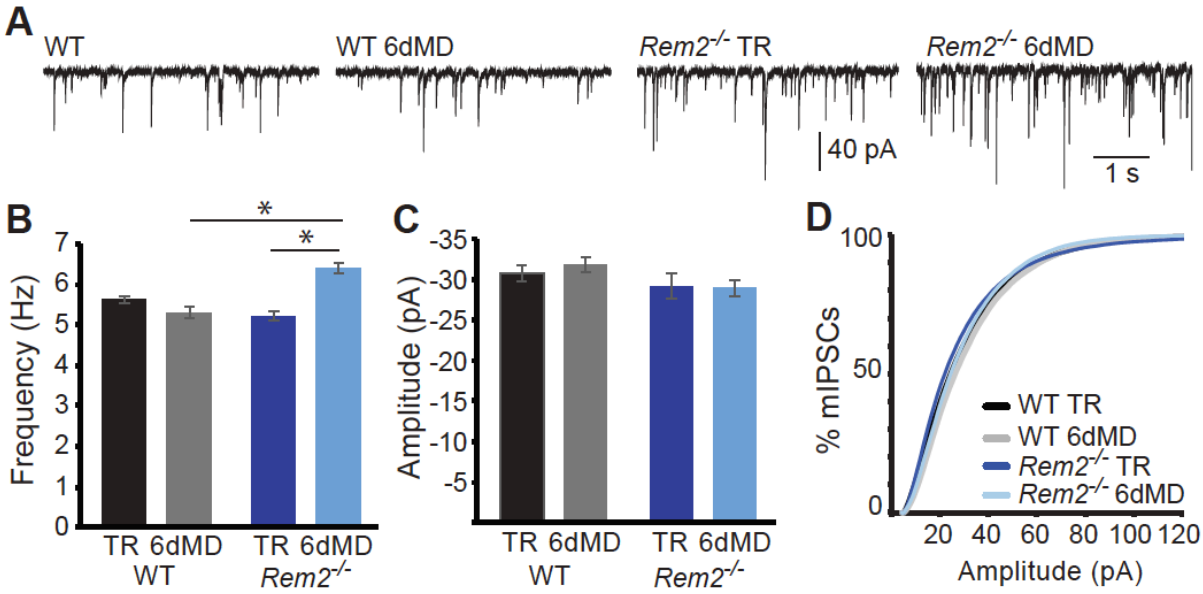

Figure S2 related to Figure 4. *Rem2*$^{-/-}$ does not alter inhibition in layer 2/3 pyramidal neurons. A) Representative whole-cell recordings of mIPSCs from layer 2/3 pyramidal neurons in V1b in wildtype or *Rem2*$^{-/-}$ that were either typically reared (TR) until P32 or monocularly deprived (from P26-P32) for 6 days (6d MD). Quantification of average mIPSC frequency (**B**) and amplitude (**C**) in WT and *Rem2*$^{-/-}$ cells (WT TR n=22, WT 6d MD n=17, *Rem2*$^{-/-}$TR n=22, and *Rem2*$^{-/-}$ 6d MD n=17). N=3 animals per condition. **D**) Cumulative distribution plot of mIPSC amplitudes in WT TR, WT 6d MD, Rem2 TR, and Rem2 MD. Data is presented as mean ± SEM. *p < 0.05 by two-way ANOVA with Tukey post-hoc.

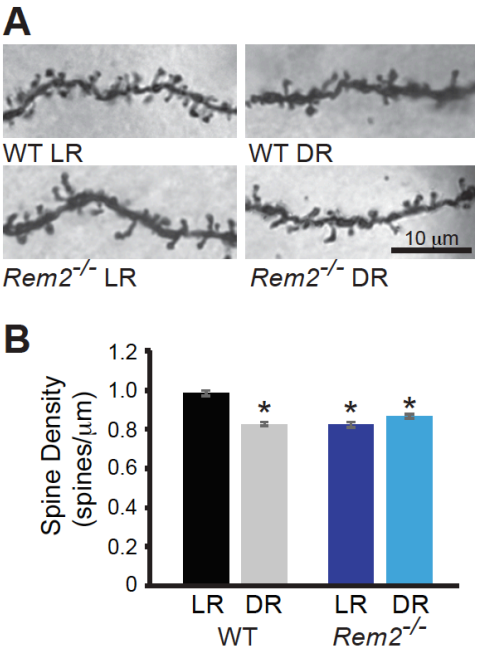

Figure S3 related to Figure 5. *Rem2*$^{-/-}$ mice exhibit decreased spine density *in vivo*. A) Representative images of Golgi-cox labeled dendritic spines. Images were taken from terminal branches off the apical tree 50-100 µm from the cell soma of layer 2/3 pyramidal neurons located in primary visual cortex. Scale bar, 10 µm. **B**) Spine density measured in wildtype and *Rem2*$^{-/-}$ mice under normal light rearing conditions (WT LR, n=29 neurons; *Rem2*$^{-/-}$ LR, n=29 neurons) or dark reared from P9-P30 (WT DR, n=36 neurons; *Rem2*$^{-/-}$ DR n=36 neurons). N=4 animals for WT LR and *Rem2*$^{-/-}$ LR and N=5 animals for WT DR and *Rem2*$^{-/-}$ DR experiments. Data is presented as mean ± SEM. * $p < 0.05$ compared to WT LR by two-way ANOVA followed by Tukey post hoc.

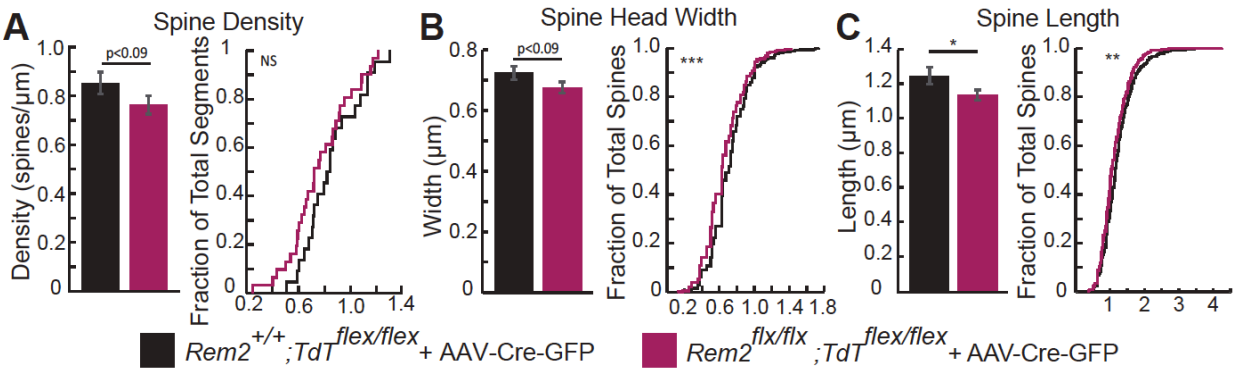

Figure S4 related to Figure 7. Brief loss of Rem2 results in a modest decrease in spine density and spine remodeling. A) Average spine density (left) and cumulative histogram of spine densities (right) for control *Rem2*$^{+/+}$;*Tdt*$^{flex/flex}$ (black, n=22) or *Rem2*$^{flx/}$*flx*;*Tdtflex*$^{/flex}$ (orange, n=31) GFP-Cre epressing neurons at 11 days post injection (d.p.i). GFP-Cre expressing neurons from *Rem2*$^{flx/flx}$*Tdt*$^{flex/flex}$ animals show a trend toward decreased mean spine density compared to control *Rem2*$^{+/+}$;*Tdt*$^{flex/flex}$ neurons (p=0.09, 2 sample t-test) and a shifit in the population of spine densities toward lower values. **B)** Average spine head width (left) and cumulative histogram (right) of spine head measurements from control *Rem2*$^{+/+}$;*Tdt*$^{flex/flex}$ (black, n=22) or *Rem2*$^{flx/flx}$;*Tdt*$^{flex/flex}$ (orange, n=31) GFP-Cre epressing neurons at 11d.p.i. GFP-Cre expressing neurons from *Rem2*$^{flx/flx}$;*Tdt*$^{flex/flex}$ mice show a trend toward decreased mean spine head width compared to control *Rem2*$^{+/+}$;*Tdt*$^{flex/flex}$ neurons (p=0.09, 2 sample t-test) and a highly significant shift in the distribution of spine head widths toward narrower spine heads (p<0.001, Kolmogorov-Smirnov test). **C)** Average spine neck length (left) and cumulative histogram (right) of spine neck measurements from control *Rem2*$^{+/+}$;*Tdt*$^{flex/flex}$ (black, n=22) or *Rem2*$^{flx/flx}$;*Tdt*$^{flex/flex}$ mice (orange, n=31) GFP-Cre epressing neurons at 11d.p.i. GFP-Cre expressing neurons from *Rem2*$^{flx/flx}$;*Tdt*$^{flex/flex}$ mice show decreased mean spine neck length compared to control *Rem2*$^{+/+}$;*Tdt*$^{flex/flex}$ (p<0.05, 2 sample t-test) and a highly significant shift in the distribution of spine head widths toward narrower spine heads (p<0.01, Kolmogorov-Smirnov test). N=5 animals per condition. Data is presented as mean ± SEM (left) and as cumulative distribution plots (right).

SUPPLEMENTAL TABLE

Statistical Comparison	Ipsi p-Value	Contra p-value
WT TR vs. WT 2d MD	0.7689	0.0149*
WT TR vs. WT 6d MD	0.2242	0.0050*
WT 2d MD vs. WT 6d MD	0.0678	0.8486
Rem2$^{-/-}$ TR vs. *Rem2*$^{-/-}$ 2d MD	0.4259	0.0031179*
Rem2$^{-/-}$ TR vs. *Rem2*$^{-/-}$ 6d MD	0.3594	0.1637101
Rem2$^{-/-}$ 2d MD vs. *Rem2*$^{-/-}$ 6d MD	0.0247*	0.1673178
WT TR vs. *Rem2*$^{-/-}$ TR	0.5419	0.5363
WT 2d MD vs. *Rem2*$^{-/-}$ 2d MD	0.7797	0.5264
WT 6d MD vs. *Rem2*$^{-/-}$ 6d MD	0.5847	0.0096*
Adult WT TR vs. Adult WT 10d MD	0.0632	0.0257*
Adult *Rem2*$^{-/-}$ TR vs. Adult *Rem2*$^{-/-}$ 10d MD	0.0598	0.6656
Adult WT TR vs. *Rem2*$^{-/-}$ TR	0.9587	0.7801
Adult WT 10d MD vs. *Rem2*$^{-/-}$ 10d MD	0.1709	0.0998
Rem2$^{+/+}$;*EMX1*^{Cre} TR vs. *Rem2*$^{+/+}$;*EMX1*^{Cre} 6d MD	0.7784	0.0440*
Rem2$^{flx/flx}$;*EMX1*^{Cre} TR vs. *Rem2*$^{flx/flx}$;*EMX1*^{Cre} 6d MD	0.9992	0.3774
Rem2$^{+/+}$;*EMX1*^{Cre} TR vs. *Rem2*$^{flx/flx}$;*EMX1*^{Cre} TR	0.9990	0.9990
Rem2$^{+/+}$;*EMX1*^{Cre} 6d MD vs. *Rem2*$^{flx/flx}$;*EMX1*^{Cre} 6d MD	0.7446	0.5876
Rem2$^{+/+}$;*PV*^{Cre} TR vs. *Rem2*$^{+/+}$;*PV*^{Cre} 6d MD	0.3275	0.2828
Rem2$^{flx/flx}$;*PV*^{Cre} TR vs. *Rem2*$^{flx/flx}$;*PV*^{Cre} 6d MD	0.7515	0.0513
Rem2$^{+/+}$;*PV*^{Cre} TR vs. *Rem2*$^{flx/flx}$;*PV*^{Cre} TR	0.9956	0.9997
Rem2$^{+/+}$;*PV*^{Cre} 6d MD vs. *Rem2*$^{flx/flx}$;*PV*^{Cre} 6d MD	0.7564	0.7999
Rem2$^{+/+}$;*VIP*^{Cre} TR vs. *Rem2*$^{+/+}$; *VIP*^{Cre} 6d MD	0.0443*	0.0875
Rem2$^{flx/flx}$; *VIP*^{Cre} TR vs. *Rem2*$^{flx/flx}$; *VIP*^{Cre} 6d MD	0.2417	0.0554
Rem2$^{+/+}$; *VIP*^{Cre} TR vs. *Rem2*$^{flx/flx}$; *VIP*^{Cre} TR	0.7063	0.7400
Rem2$^{+/+}$; *VIP*^{Cre} 6d MD vs. *Rem2*$^{flx/flx}$; *VIP*^{Cre} 6d MD	0.5437	0.3990

Table S1 related to Figures 3 and 4. Statistical comparisons of Individual Eye Responses as measured for ocular dominance index. Statistical comparisons of Changes in reflectance over baseline reflectance (ΔR/R) for ipsilateral (I) or contralateral (C) eye response vales for wildtype and *Rem2* deletion mice as measured by intrinsic signal imaging. These values correspond to the ΔR/R values displayed in Fig. 3C-D and Fig. 4 insets. *$p \leq 0.05$ by a two-way ANOVA followed by a Tukey test. All other comparisons are not significant.

Experimental Condition	V_R (mV)	R_{IN} (GΩ)	C_M (pF)	Tau (ms)
WT TR	-68.01 ± 0.43	95.09 ± 1.56	113.98 ± 1.70	10.78 ± 0.21
WT 2d MD	-66.78 ± 0.38	96.46 ± 2.11	108.84 ± 2.48	10.12 ± 0.15
Rem2$^{-/-}$ TR	-64.98 ± 0.26	111.61 ± 1.80	105.50 ± 1.95	11.44 ± 0.16
Rem2$^{-/-}$ 2d MD	-68.38 ± 0.38$^{\#}$	100.94 ± 2.25	109.70 ± 2.72	10.79 ± 0.27
WT TR	-64.22 ± 0.23	104.15 ± 1.64	118.55 ± 1.97	12.03 ± 0.15
WT 6d MD	-64.92 ± 0.19	109.38 ± 1.10	119.94 ± 1.46	10.77 ± 0.10$^{\#}$
Rem2$^{-/-}$ TR	-63.39 ± 0.43	112.06 ± 1.62	124.80 ± 2.15	13.86 ± 0.29
Rem2$^{-/-}$ 6d MD	-64.38 ± 0.19	99.61 ± 1.34	125.31 ± 1.61	11.96 ± 0.15
4 days post infection				
Rem2$^{flx/flx}$ +AAV-GFP	-67.48 ± 0.54	108.88 ± 3.81	101.69 ± 2.35	11.26 ± 0.35
Rem2$^{flx/flx}$ +AAV-GFP-CRE	-69.38 ± 0.59	101.26 ± 2.68	96.75 ± 2.59	9.66 ± 0.31
10-12 days post infection				
Rem2$^{flx/flx}$ +AAV-GFP	-64.04 ± 0.56	105.87 ± 3.75	111.54 ± 3.62	11.35 ± 0.39
Rem2$^{flx/flx}$ +AAV-GFP-CRE	-64.21 ± 0.44	122.07 ± 3.10	102.56 ± 2.42	12.30 ± 0.37

Table S2 related to Figure 7. Passive membrane properties of layer 2/3 neurons in visual cortex. Passive membrane properties including resting membrane potential (V_R), input resistance (R_{IN}), membrane capacitance (C_M), and Tau measured in layer 2/3 pyramidal neurons in wildtype and *Rem2*$^{-/-}$ TR or MD mice for the cells assayed in Figure 7. *$p \leq 0.05$ compared to WT TR or $^{\#}p \leq 0.05$ compared to *Rem2*$^{-/-}$ TR by a two-way ANOVA followed by a Tukey test. All other comparisons are not significant. For *Rem2*$^{flx/flx}$ mice, data is compared using an independent student's *t*-test.